Supplemental Document

optica

Petahertz-scale nonlinear photoconductive sampling in air: supplement

Dmitry Zimin,[1,2] Matthew Weidman,[1,2,4] Johannes Schötz,[1,2] Matthias F. Kling,[1,2] Vladislav S. Yakovlev,[1,2] Ferenc Krausz,[1,2] and Nicholas Karpowicz[1,3,*]

[1]*Max-Planck-Institut für Quantenoptik, Hans-Kopfermann-Strasse 1, 85748 Garching, Germany*
[2]*Fakultät für Physik, Ludwig-Maximilians-Universität, Am Coulombwall 1, 85748 Garching, Germany*
[3]*CNR NANOTEC Institute of Nanotechnology, via Monteroni, 73100 Lecce, Italy*
[4]*e-mail: matthew.weidman@mpq.mpg.de*
[*]*Corresponding author: nicholas.karpowicz@nanotec.cnr.it*

Supplement DOI: https://doi.org/10.6084/m9.figshare.14141741

Parent Article DOI: https://doi.org/10.1364/OPTICA.411434

Non-linear photoconductive sampling at near-PHz frequencies in air: supplemental document

Experimental setup

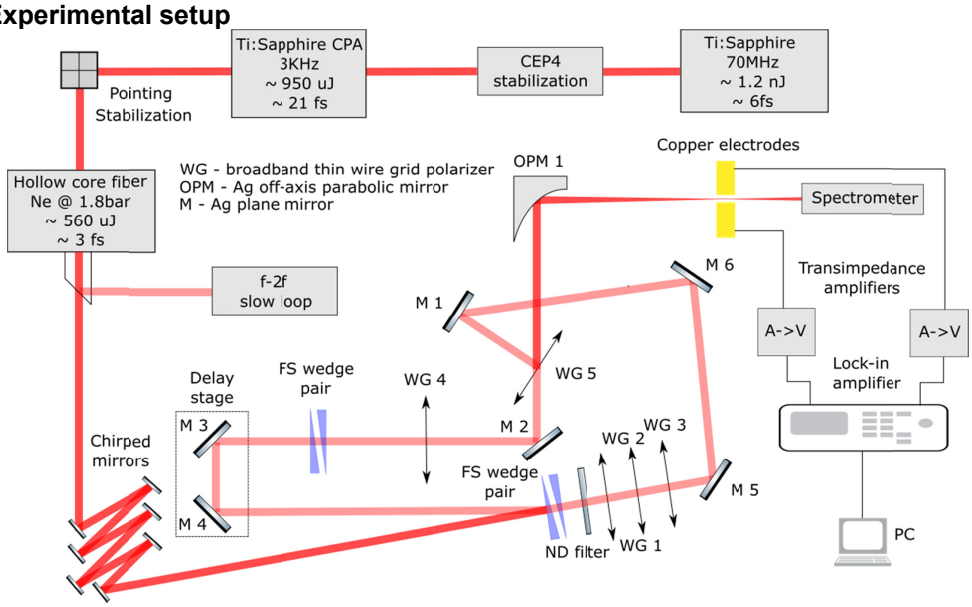

Fig. S1. Experimental setup

A Ti:sapphire oscillator (Rainbow 2, Spectra Physics) was used to provide an octave-spanning bandwidth with carrier-envelope phase (CEP)-stabilization achieved using a feed-forward scheme (Fig. S1). The pulses were amplified using a 9-pass cryo-cooled Ti:sapphire chirped pulse amplifier at a repetition rate of 3 kHz, and temporally compressed using a transmission grating based compressor, yielding 21 fs pulses with 2.5 W average output power. The amplified pulses were spectrally broadened in a hollow core fiber (HCF), filled with 1.8 bar neon gas and compressed to 2.6 fs FWHM. The pulse width is based on the intensity envelope of the complex-valued analytic wave, whose real part is the electric field measured by NPS, and the imaginary part is the Hilbert transform of the field. This definition of the pulse width is independent of carrier envelope phase. The compression is achieved using three pairs of chirped mirrors. The pulses were separated into two arms, by taking a reflection from the front surface of a wedge. In each arm, the final compression and CEP were adjusted by a pair of fused silica wedges [1]. The pulse energies and polarizations were controlled by a set of wire-grid polarizers (WG1 - WG4), in order to prevent reshaping of pulses and beam parameters caused by irises.

Both arms were delayed with respect to each other using a retro-reflector (M3 and M4) placed on a closed-loop piezo stage (PX 200, Piezosystems Jena). Finally, both arms were recombined using a wire-grid polarizer WG5, which transmits one arm and reflects another. These two pulses, dubbed “injection” and “drive” were polarized 90 degrees to one another,

and focused inside the gap between electrodes using an off-axis parabolic mirror with an effective focal length of 152 mm. The focus of both pump and injection beams was measured to be 78 μm full-width at $1/e^2$. The gap between electrodes was adjusted to match the size of the focal spots, and is approximately 80 μm.

The stronger pulse, which was vertically polarized, injected carriers. Because the injection pulse was polarized along the direction of the electrodes, it did not by itself displace the created charges towards electrodes. The second, weaker "drive" pulse was polarized across the electrodes and was responsible for the displacement of charges created by the injection pulse. The displaced charge creates a dipole which is further shielded by an opposing electric field on a metal. The created potential on electrodes generates a measurable current from/to electrodes to/from a ground. A transimpedance amplifier was used to provide a voltage in response to an input current. Both electrodes were connected to a lock-in amplifier (Stanford research systems SR830). To avoid non-coherent background noise caused by heating of metal electrodes by a laser pulse, the CEP of every second pulse was changed by pi and the trigger at the half of the repetition rate of the laser was used for the lock-in detection. The lock-in amplifier was interfaced with a computer for the data acquisition.

For the case of the waveform sampling in of an infrared spectrum centered at about 2 μm, mirrors M5 and M6 where replaced with off-axis parabolic mirrors of equal focal lengths in order to create an intermediate focal plane in between. A Beta barium borate (BBO) crystal of type II was placed in the intermediate focal plane for the intra-pulse difference frequency generation, followed by a set of silicon and fused silica plates to block the fundamental spectrum and compress the generated infrared pulse.

Infrared measurement

The NPS technique is intrinsically broadband, as was demonstrated previously in the case of solids. In Figure S2, we show that the there is also a response in air in the infrared. A phase-stable field in the spectral range from 120-200 THz was generated through intra-pulse difference frequency generation (iDFG) [2] by placing a BBO crystal in the drive arm of the interferometer. The pulse has a smaller fractional bandwidth compared to the measurements in the visible, which allows for a confirmation that the signal is free of harmonic distortions above the measurement noise floor within the range of drive field strengths measured.

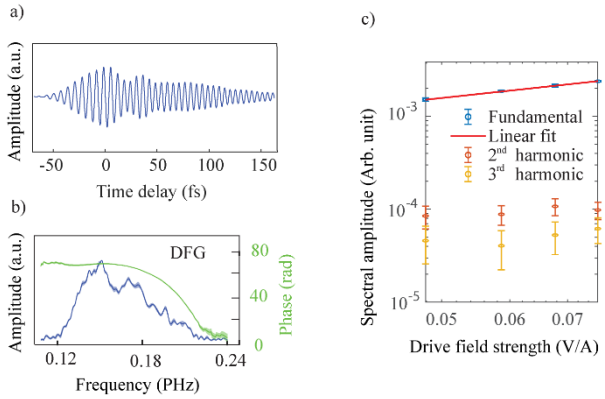

Fig. S2. Measured waveform (a) and retrieved spectrum (b) of 2 μm pulses generated through iDFG.(c) Scaling of the signal as a function at the fundamental and harmonics of the drive field strength, indicating that the signal is free of harmonic distortions in the measured range of intensities. The injection field strength was 0.8 V/Å.

Numerical simulations

The time dependent Schrödinger equation was solved numerically in the velocity gauge following the algorithm introduced by Muller [3] to produce the results displayed in Figures 1 and 3. The simulation is three-dimensional, as is required by the cross-polarized configuration of the electric fields. The simulation grid comprises a set of partial radial waves, corresponding to the quantum numbers ℓ and m. This basis of radial position and angular momentum is rather efficient for numerical solution of the TDSE in a radially-symmetric potential, as the quantization in the two momentum axes is exact. The grid resolution in the radial direction is 0.2 atomic units, and the time step is 2.5 attoseconds. At each time step, the system of coordinates is rotated such that the vector potential of the incident laser field is aligned to the z-axis (such that the laser field does not couple partial waves of different m), rotating the wavefunction with the rotation operator constructed from the angular momentum operators. The polarization angle does not change monotonically in time, so no small-angle approximations are applied to the operator.

The electron spectra are calculated by projecting the wavefunction at the end of the simulation (after the vector potential and electric field are both zero) onto free electron scattering states obtained by solution of the static Schrödinger equation in the same system. Care must be taken here to obtain accurate Coulomb phases $\phi_{k,\ell}$, which is done by extension of the radial grid to 8000 atomic units and performing a single parameter least squares fitting of the numerically obtained waveform to the asymptotic form

$$\psi_{k,\ell} \approx sin\left(kr + Z\,log(2kr)/k + \phi_{k,\ell}\right)/r. \#(1)$$

The projections are performed as a function of angle and momentum to produce the angularly-resolved photoelectron spectra. The momentum asymmetry, taken to be an estimate of the experimental signal, is obtained by calculating a complete set of spectra in the x-z plane and taking the expectation value of the momentum in the x-direction (in the coordinate

system of the simulation, the injection field points along the z-axis, and the drive field along the x-axis).

Two spherically-symmetric potentials were used for simulations: a standard Coulomb potential, $V = -1/r$ for the case of hydrogen, and a spherical quantum well of the form

$$V = -2.4276e^{-r^4/2}, \#(2)$$

which has only one bound state of 13.6 eV binding energy, and rapidly reaches zero away from the origin, resulting in a short-range potential. The desired eigenenergy and number of states may easily be obtained in such a potential by adjusting its depth and width.

In simulating the response function of the measurement as depicted in Fig. 3 of the main text, we calculate the response for the pulse where the signal is optimal, and for the pulse where it is minimized. The expected time-domain traces that would appear directly in the measurement are shown in Fig. S3.

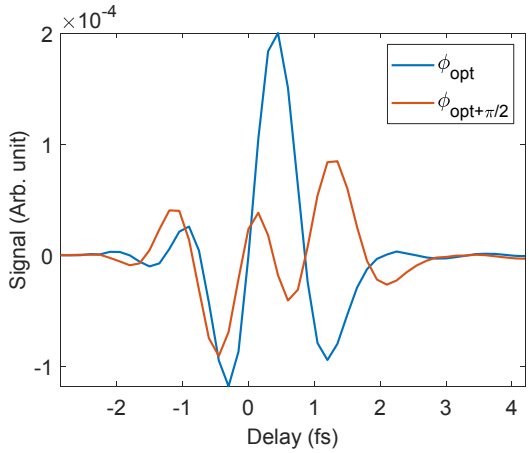

Fig. S3. Simulated waveforms corresponding to the values of injection pulse CEP that minimize and maximize the signal in the experiment, corresponding to the optimally flat and most distorted spectral responses respectively. Experimentally, optimizing the CEP of the injection pulse to provide the largest signal also maximally compresses and simplifies the gate.

Supplementary References

1. Paasch-Colberg, T., A. Schiffrin, N. Karpowicz, S. Kruchinin, Ö. Sağlam, S. Keiber, O. Razskazovskaya, S. Mühlbrandt, A. Alnaser, and M. Kübel, *Solid-state light-phase detector.* Nature Photonics, 2014. **8**(3): p. 214-218.

2. Fattahi, H., A. Schwarz, S. Keiber, and N. Karpowicz, *Efficient, octave-spanning difference-frequency generation using few-cycle pulses in simple collinear geometry.* Optics Letters, 2013. **38**(20): p. 4216-4219.
3. Muller, H., *An efficient propagation scheme for the time-dependent Schrodinger equation in the velocity gauge.* Laser Physics, 1999. **9**(1): p. 138-148.